Improved design of a high-voltage vacuum-insulator interface

W. A. Stygar,[1] J. A. Lott,[2] T. C. Wagoner,[2] V. Anaya,[2] H. C. Harjes,[1] H. C. Ives,[3] Z. R. Wallace,[2] G. R. Mowrer,[1] R. W. Shoup,[1] J. P. Corley,[2] R. A. Anderson,[1] G. E. Vogtlin,[4] M. E. Savage,[1] J. M. Elizondo,[1] B. S. Stoltzfus,[1] D. M. Andercyk,[5] D. L. Fehl,[1] T. F. Jaramillo,[2] D. L. Johnson,[6] D. H. McDaniel,[1] D. A. Muirhead,[1] J. M. Radman,[5] J. J. Ramirez,[1] L. E. Ramirez,[2] R. B. Spielman,[1] K. W. Struve,[1] D. E. Walsh,[7] E. D. Walsh,[7] and M. D. Walsh[7]

[1]*Sandia National Laboratories, Albuquerque, New Mexico 87185, USA*
[2]*Ktech Corporation, Albuquerque, New Mexico 87123, USA*
[3]*EG&G, Albuquerque, New Mexico 87107, USA*
[4]*Lawrence Livermore National Laboratory, Livermore, California 94550, USA*
[5]*Trace Laboratories, Hunt Valley, Maryland 21030, USA*
[6]*Titan-Pulse Sciences Division, San Leandro, California 94577, USA*
[7]*C-Lec Plastics, Philadelphia, Pennsylvania 19135, USA*

(Received 26 November 2004; published 12 May 2005)

We have conducted a series of experiments designed to measure the flashover strength of various azimuthally symmetric 45° vacuum-insulator configurations. The principal objective of the experiments was to identify a configuration with a flashover strength greater than that of the standard design, which consists of a 45° polymethyl-methacrylate (PMMA) insulator between flat electrodes. The thickness d and circumference C of the insulators tested were held constant at 4.318 and 95.74 cm, respectively. The peak voltage applied to the insulators ranged from 0.8 to 2.2 MV. The rise time of the voltage pulse was 40–60 ns; the *effective* pulse width [as defined in Phys. Rev. ST Accel. Beams **7**, 070401 (2004)] was on the order of 10 ns. Experiments conducted with flat aluminum electrodes demonstrate that the flashover strength of a crosslinked polystyrene (Rexolite) insulator is $(18 \pm 7)\%$ higher than that of PMMA. Experiments conducted with a Rexolite insulator and an anode plug, i.e., an extension of the anode into the insulator, demonstrate that a plug can increase the flashover strength by an additional $(44 \pm 11)\%$. The results are consistent with the Anderson model of anode-initiated flashover, and confirm previous measurements. It appears that a Rexolite insulator with an anode plug can, in principle, increase the peak electromagnetic power that can be transmitted across a vacuum interface by a factor of $[(1.18) \times (1.44)]^2 = 2.9$ over that which can be achieved with the standard design.

DOI: 10.1103/PhysRevSTAB.8.050401 PACS numbers: 84.70.+p, 77.22.Jp, 52.80.−s, 52.90.+z

I. INTRODUCTION

Experiments conducted on pulsed-power and particle accelerators typically require that a high-voltage pulse be transmitted across a vacuum-insulator interface. Since 1964, the standard interface for pulsed applications has consisted of a 45° polymethyl-methacrylate (PMMA) insulator between flat electrodes, or several such systems connected in series [1–36]. (A cylindrical configuration of several insulators in series is often referred to as an insulator stack [1,14–17,32,36–44].) Because of various technical considerations, it is usually desired to minimize the distance at the interface over which the voltage is applied; hence it is of interest to develop an interface with a flashover strength greater than that of the standard design.

Experiments and observations described in the literature suggest that the flashover of a 45° interface is most likely to initiate at the anode triple junction, i.e., at the intersection of the anode, insulator, and vacuum regions [1,8–10,13,20,22,25,26]. In Secs. II A, II B, and II C, we present numerical and analytic calculations which show that the electric field on the vacuum side of a 45° interface, and that inside the bulk insulator material, are highest at the anode junction. The field is enhanced at the junction by the 45° geometry and the dielectric mismatch at the vacuum-insulator interface.

A model of anode-initiated flashover has been developed by Anderson [8–10,13,25]. We review the model in Sec. II D. The mechanism proposed by Anderson can be summarized as follows: At a sufficiently high voltage, the flashover of a 45° interface initiates at the anode junction due to emission of electrons from the insulator [1,8–10,13,25,45,46]. The emission increases the electric field at the insulator surface, which in turn precipitates bulk-dielectric-breakdown events at the surface. The events branch across the surface until they reach the cathode and the flashover is complete.

The calculations presented in Sec. II show that the electric field near the anode junction *increases* as the insulator's dielectric constant ε is increased, and that the field near the cathode junction *decreases* as ε is increased. Hence assuming the Anderson model, we expect that *when all other insulator properties are held constant*, the flashover strength of an insulator would decrease as ε increases. We also expect that the flashover strength would be an increasing function of the insulator's bulk-dielectric-breakdown strength.

Seminal experiments conducted by Milton [5,7], Roth and co-workers [33], and Vogtlin and co-workers [20,22,26] are consistent with these expectations. Milton tested a number of insulator materials with ε that ranges from 2 to ~3000, and finds that *in general*, the flashover strength decreases as ε increases [5,7]. Milton [5,7] and Roth *et al.* [33] also find that crosslinked polystyrene (Rexolite) has a flashover strength comparable to or greater than that of PMMA. This is as expected, since as discussed in Sec. II, Rexolite has a smaller dielectric constant and a higher bulk-dielectric-breakdown strength.

The results obtained by Milton [5,7] and Roth and co-workers [33] suggest that the flashover of a 45° insulator is *not* likely to initiate at the cathode triple junction, since if this were the case, the flashover strength would *increase* as ε is increased. This observation is consistent with experiments conducted by Vogtlin, Hofer, and Wilson [20], which show that when the insulator material is held constant, and shaped electrodes are used to *reduce* the cathode-junction field and *increase* the field at the anode junction, the flashover strength is *reduced*.

Vogtlin and co-workers [20,22,26] also conducted experiments with a 45° insulator and an anode plug, i.e., an extension of the anode into the insulator. The plug was designed to serve as a partial Faraday cage around the anode triple junction, to deenhance the junction's electric field. The measurements described in Ref. [20] demonstrate that an anode plug can increase the flashover strength of a 45° Lexan insulator by at least 38%. (The use of an anode plug was first proposed by McDaniel in 1975 [47], as discussed briefly by Anderson in Ref. [9].) Electric-field calculations of an insulator with an anode plug are presented in Sec. II E. The calculations verify that a plug can significantly reduce the field at the anode junction, as first demonstrated by Vogtlin, Hofer, and Wilson [20].

Motivated by the Anderson model and the results described by Milton [5,7], Roth *et al.* [33], and Vogtlin *et al.* [20,22,26], we have conducted a series of controlled flashover experiments to validate that the flashover strength of a 45° vacuum-insulator interface can be improved as indicated. The experiments were conducted with insulators at least a factor of 2.7 thicker, and a factor of 6.4 larger in circumference, than those described in Refs. [5,7,20,22,26,33]. We have also conducted the first anode-plug experiments with a Rexolite insulator. Our results confirm the previous observations [5,7,20,22,26,33]; i.e., we find that for the conditions studied, the flashover strength of a 45° interface can be improved as predicted by the Anderson model.

The experimental arrangement used, and the various 45° insulator-electrode configurations studied, are described in Sec. III. Results are summarized in Sec. IV. In Sec. V, we discuss limitations of the use of Rexolite and an anode plug, and present suggestions for future work.

II. THEORY

A. 2D electric field of a 45° vacuum-insulator interface

The standard 45° vacuum-insulator interface, first tested under pulsed conditions by Smith [1], has been used for pulsed-power applications since 1964 [1–36]. This interface consists of a flat anode, a flat cathode, and a PMMA insulator with a 45° vacuum-insulator interface. An idealized two-dimensional (2D) 45° interface is illustrated in Fig. 1. By convention, the interface outlined in Fig. 1 is referred to as a 45° system. In a −45° system, the bottom electrode of Fig. 1 would be the anode.

As indicated by the figure, the anode triple junction (atj) is the point at which the vacuum, insulator, and anode regions meet. The cathode triple junction (ctj) is similarly defined.

Results of 2D electrostatic-field calculations for the idealized geometry of Fig. 1 are presented in Figs. 2 and 3. These and all other numerical electric-field calculations described in this article were performed with ELECTRO [48], which uses a boundary-element (Green-function) method to calculate the electric field. The number and distribution of the boundary elements along the insulator and electrode surfaces were determined by ELECTRO's self-adaptive solver. For each calculation that was performed, the number of elements was increased by the solver until the boundary conditions were satisfied to within 0.05%.

The calculations presented in Figs. 2 and 3 assume that the insulator and electrodes extend infinitely both into and out of the page, and that the insulator has a relative dielectric constant ε of 2.55. As indicated by Table I, this is the average value for Rexolite at frequencies between 100 kHz and 1 GHz. The fields presented in Figs. 2 and 3 are similar to those that would be obtained with PMMA, for which (as indicated by Table I) the average value of ε is 2.92. We assume $\varepsilon = 2.55$ for these figures since most of the experiments discussed in Secs. III, IV, and V use Rexolite.

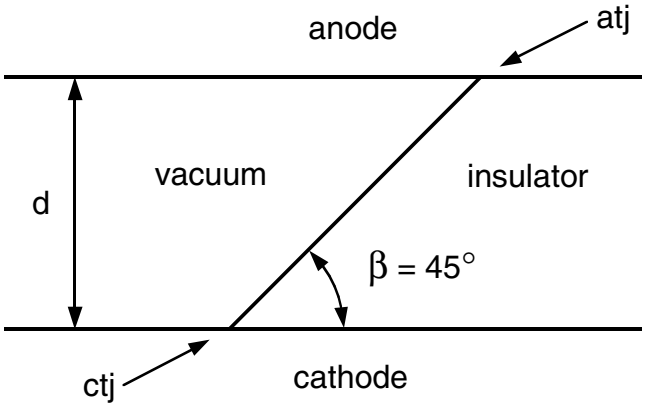

FIG. 1. Idealized 2D 45° vacuum-insulator interface. The anode triple junction (atj) is the point at which the vacuum, insulator, and anode regions meet; the cathode triple junction (ctj) is similarly defined.

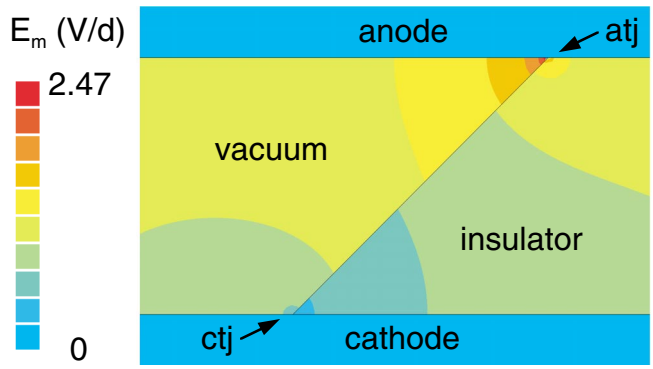

FIG. 2. (Color) The absolute value of the electric-field magnitude E_m as a function of position for the idealized 45° vacuum-insulator interface outlined in Fig. 1. The calculation assumes that the dielectric constant of the insulator $\varepsilon = 2.55$. The anode triple junction (atj) is the point at which the vacuum, insulator, and anode regions meet; the cathode triple junction (ctj) is similarly defined. The color legend is a linear scale. The field is given in units of V/d, where V is the voltage across the insulator and d is the insulator thickness as defined by Fig. 1.

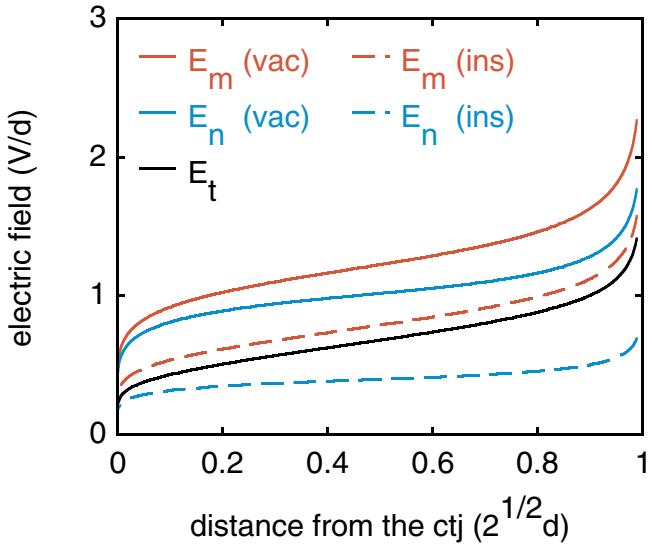

FIG. 3. (Color) Electric fields as a function of distance along the vacuum-insulator interface of the idealized 45° insulator-electrode system outlined in Figs. 1 and 2. The plots assume that the dielectric constant of the insulator $\varepsilon = 2.55$. The quantity E_n is the absolute value of the electric field normal to the interface, E_t is the absolute value of the field tangent to the interface, and $E_m = (E_n^2 + E_t^2)^{1/2}$. The fields are given in units of V/d, where V is the voltage across the insulator and d is the insulator thickness as defined by Fig. 1. The distance from the ctj is given in units of $2^{1/2}d$, the total length of the interface.

Figure 2 displays the absolute value of the electric-field magnitude E_m as a function of position. Figure 3 plots (as a function of distance along the vacuum-insulator interface) the following quantities: the field magnitude E_m; the absolute value of the electric-field component normal to the interface E_n; and the absolute value of the tangential component E_t. The fields on both the vacuum and insulator sides of the interface are plotted; on both sides $E_m = (E_n^2 + E_t^2)^{1/2}$. The fields are plotted in units of the mean electric field, which we define as V/d, where V is the voltage across the insulator and d is the insulator thickness as defined by Fig. 1. [For example, when $V = 500$ kV and $d = 5$ cm, the peak value of E_m in Fig. 2 would be $(2.47V/d) = 247$ kV/cm.] The distance from the ctj given

TABLE I. Measured values of the dielectric constant ε, dielectric strength, and water absorption of polymethyl methacrylate (acrylic 100M) and crosslinked polystyrene (Rexolite 1422). The measurements were performed at room temperature. Each set of measurements was performed on 5 samples; the uncertainty given is the standard deviation of the mean due to random fluctuations [49]. The dielectric-strength measurements were performed under oil (to prevent flashover) on samples that were nominally 0.29 mm thick. The voltage applied was at 60 Hz, and was increased on each sample at 500 V (rms) per second until breakdown occurred. The breakdown fields reported in the table are rms values.

Insulator property	Testing method	Polymethyl methacrylate (acrylic 100M)	Crosslinked polystyrene (Rexolite 1422)
ε (100 kHz)	ASTM-D-150-98 ASTM-D-2520-01	2.802 ± 0.008	2.546 ± 0.004
ε (1 MHz)	ASTM-D-150-98 ASTM-D-2520-01	3.070 ± 0.008	2.546 ± 0.002
ε (10 MHz)	ASTM-D-150-98 ASTM-D-2520-01	2.984 ± 0.007	2.546 ± 0.005
ε (100 MHz)	ASTM-D-150-98 ASTM-D-2520-01	2.910 ± 0.005	2.544 ± 0.004
ε (1 GHz)	ASTM-D-150-98 ASTM-D-2520-01	2.846 ± 0.002	2.546 ± 0.002
Dielectric strength	ASTM-D-149-97a	556 ± 7 kV/cm	819 ± 21 kV/cm
Water absorption	ASTM-D-570-98	(0.328 ± 0.002)%	(0.054 ± 0.002)%

in Fig. 3 is in units of $2^{1/2}d$, the length of the vacuum-insulator interface.

Figures 2 and 3 show that for the standard 45° geometry, the electric field is significantly enhanced at the anode triple junction. (This geometric enhancement is well known; please see, for example, Refs. [1,20,50].) The absolute value of the electric-field magnitude on the vacuum side of the anode junction is higher than anywhere else in the system. The electric field on the insulator side of the junction is higher than anywhere else inside the insulator material.

B. Analytic scaling of the anode- and cathode-triple-junction fields

The fields presented in Figs. 2 and 3 were obtained numerically. As demonstrated by Schächter [51] and Chung *et al.* [52], the functional dependence of the electric field on the distance from either an anode or cathode junction can be obtained analytically.

For the geometry shown in Fig. 1, the angle $\beta = 45°$. We label this angle β to be consistent with the notation adopted in Ref. [52]. (In the pulsed-power community, the insulator angle for a vacuum-insulator interface is usually defined as $90° - \beta$. Hence when $\beta = 45°$ as in Fig. 1, the insulator is said to be at 45°; when $\beta = 135°$, the insulator is said to be at $-45°$.)

The results obtained in Refs. [51,52] assume an idealized 2D triple junction, with perfect planar interfaces and infinitely sharp corners. Under these conditions, when $\varepsilon > 1$, then for all β such that $0° < \beta < 90°$, the field precisely at the cathode triple junction equals 0, and the field at the anode junction is infinite. Similarly when $\varepsilon > 1$, then for all β such that $90° < \beta < 180°$, the field at the cathode junction is infinite, and the anode-junction field equals 0. (Such infinite fields are, of course, mathematical abstractions achieved at idealized junctions, and would not be obtained with real materials.) When β is exactly equal to 90°, the field at the anode and cathode triple junctions are identical, and are equal to the mean field V/d.

Specifically, the absolute value of the electric-field magnitude E_m near a 2D vacuum-insulator-metal triple junction (with arbitrary angles for the vacuum, insulator, and metal regions) can be expressed as follows [52]:

$$E_m = Kr^{\nu-1}, \tag{1}$$

where K and ν are constants, and r is the distance from the junction. The constant K is a function of the system geometry, total applied voltage, and ε, and differs for the anode and cathode junctions. K also depends on whether the field being considered is on the vacuum or insulator side of the junction. Equation (1) assumes a steady-state system, and that there is no field inside the metal. This equation is applicable only when r is much less than other characteristic dimensions of the insulator-electrode system, such as d.

For the anode triple junction of the geometry shown in Fig. 1, υ is determined by the following transcendental equation [51,52]:

$$\varepsilon = \frac{-\tan(3\upsilon\pi/4)}{\tan(\upsilon\pi/4)}. \tag{2}$$

For the cathode triple junction of Fig. 1, υ is determined by [51,52]

$$\varepsilon = \frac{-\tan(\upsilon\pi/4)}{\tan(3\upsilon\pi/4)}. \tag{3}$$

As indicated by Eqs. (2) and (3), when $\varepsilon = 1$, then $\upsilon = 1$ for both the anode and cathode junctions. In this case, since there is no dielectric mismatch between the insulator and vacuum regions, there is no field enhancement at the anode, and no deenhancement at the cathode. When $\varepsilon > 1$, then according to Eq. (2), $\upsilon < 1$ for the anode junction, and according to Eq. (3), $\upsilon > 1$ for the cathode junction.

Figure 4 plots υ as a function of ε for both the anode and cathode junctions. As indicated by the figure, for the anode junction $\upsilon \leq 1$, and υ decreases as ε increases. Hence as $r \rightarrow 0$, E_m goes more rapidly to infinity (i.e., is more *enhanced*) as ε increases. For the cathode junction $\upsilon \geq 1$, and υ increases as ε increases. Hence as $r \rightarrow 0$, E_m goes more rapidly to 0 (i.e., is more *deenhanced*) as ε increases.

According to Eq. (2), when $\varepsilon = 2.55$, then $\upsilon = 0.8599$. Hence assuming Eq. (1), we expect that near the anode junction $E_m \propto r^{-0.1401}$. Figure 5 compares this analytic scaling to the numerical calculation of E_m at the interface, on the vacuum side. [The numerical calculation of E_m plotted in Fig. 5 is identical to that labeled E_m (vac) in Fig. 3.] The analytic relation is normalized to the numerical

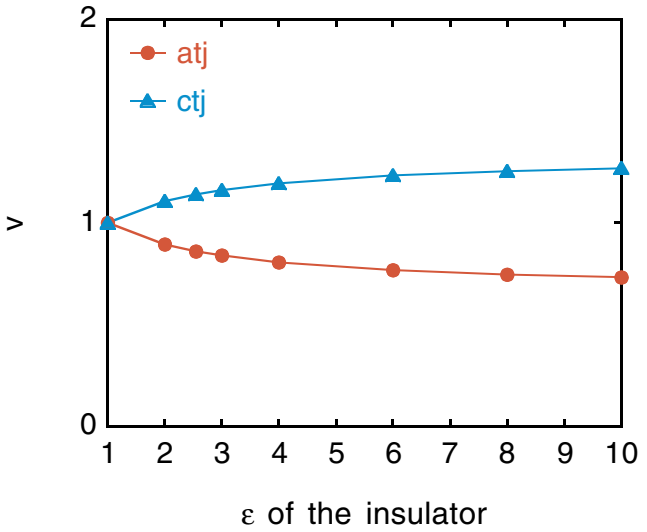

FIG. 4. (Color) The quantity υ as a function of ε for the idealized 45° vacuum-insulator system outlined in Figs. 1 and 2. The absolute value of the electric-field magnitude E_m near either an anode or cathode triple junction (atj or ctj) is proportional to $r^{\upsilon-1}$, where r is the distance from the junction [51,52].

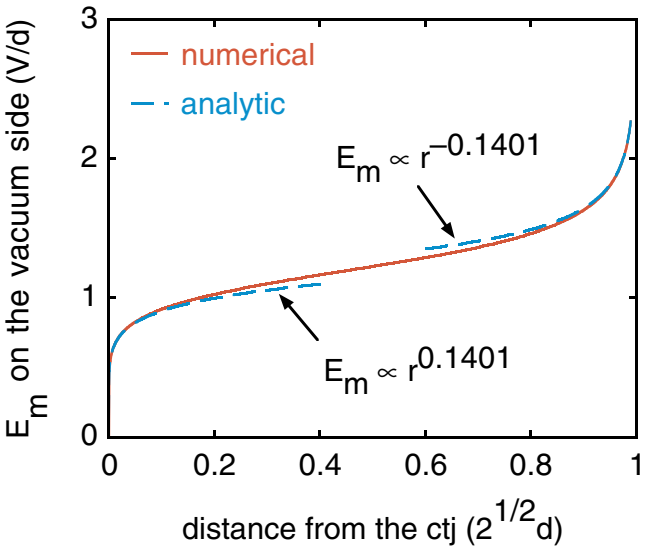

FIG. 5. (Color) The absolute value of the electric-field magnitude E_m as a function of distance along the vacuum-insulator interface of the idealized 45° system outlined in Figs. 1 and 2. The field is that on the vacuum side of the interface, and assumes that the dielectric constant of the insulator $\varepsilon = 2.55$. The plots compare the field obtained numerically with those given analytically by Eqs. (1)–(3). [The numerical result is identical to that labeled E_m (vac) in Fig. 3.] The relation $E_m \propto r^{-0.1401}$ is normalized to the numerical result at a distance $0.01(2^{1/2}d)$ from the anode triple junction; the relation $E_m \propto r^{0.1401}$ is normalized at a distance $0.01(2^{1/2}d)$ from the cathode junction.

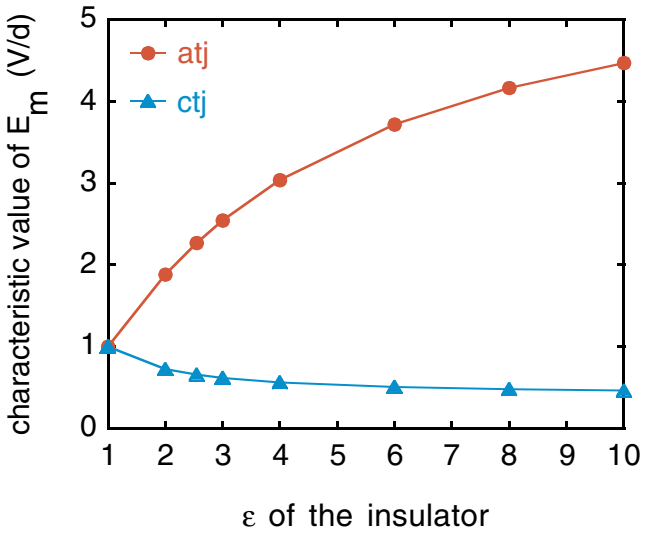

FIG. 6. (Color) The characteristic value of E_m near the anode and cathode triple junctions for the idealized 45° vacuum-insulator interface outlined in Figs. 1 and 2. Plotted is the field on the vacuum side of the interface as a function of the dielectric constant ε. We arbitrarily define the characteristic field to be that at the interface, at a distance $(0.01)2^{1/2}d$ from a junction.

result at a distance $0.01(2^{1/2}d)$ from the anode junction. The analytic scaling is consistent to within 2% with the numerical result for distances within $0.2(2^{1/2}d)$ of the anode junction.

According to Eq. (3), when $\varepsilon = 2.55$, then $\upsilon = 1.1401$. Hence near the cathode junction, Equation (1) predicts that $E_m \propto r^{0.1401}$. This analytic relation is also plotted in Fig. 5, and is normalized to the numerical result at a distance $0.01(2^{1/2}d)$ from the cathode junction. The analytic scaling is consistent to within 3% with the numerical result for distances within $0.2(2^{1/2}d)$ of the cathode junction.

C. Characteristic triple-junction fields

As discussed in Sec. II B, the absolute value of the electric-field magnitude E_m at the anode junction for the geometry of Fig. 1 is infinite for all $\varepsilon > 1$. However, this applies only precisely at the junction. We are also interested in the field in the *vicinity* of the junction, i.e., the field that extends over a nonzero area of the insulator, since this may be more relevant to insulator flashover.

For this article, we define the *characteristic* value of E_m near either an anode or cathode junction to be the field on the vacuum-insulator interface, at a distance $(0.01)(2^{1/2}d)$ from the junction. Hence the characteristic field is that at a distance 1% of the length of the interface away from a junction. The choice of 1% is arbitrary, and is used only to provide a consistent estimate of the field near an ideal triple junction, at which the field is either zero or infinite.

Figure 6 plots (as a function of ε) the characteristic value of E_m, on the vacuum side of the interface, for both the anode and cathode junctions of the configuration illustrated in Figs. 1 and 2. The fields were obtained from numerical 2D electrostatic-field calculations. As the figure shows, the characteristic value of E_m near the anode junction *increases* as ε is increased; the characteristic value of E_m near the cathode junction *decreases* with increasing ε.

D. Anderson model of anode-initiated flashover

If the flashover of a 45° insulator initiates at the *anode* triple junction, then Figs. 4 and 6 suggest that the flashover strength should *decrease* as ε is increased. Alternatively, Figs. 4 and 6 suggest that if the flashover initiates at the *cathode* junction, then the flashover strength should *increase* as ε is increased.

Experiments conducted by Milton [5,7] and Roth *et al.* [33] demonstrate that the flashover strength decreases as ε is increased, which suggest that the flashover of a 45° interface most likely initiates at the anode. Experiments conducted by Vogtlin *et al.* [20,22,26] with shaped electrodes, and other flashover measurements [1,8–10,13], also suggest an anode-initiated process. These results [1,5,7–10,13,20,22,26,33] are consistent with Figs. 2 and 3, which show that the electric field is enhanced at the anode junction. (We caution that in all these cases, we are comparing the results of pulsed flashover measurements to static electric-field calculations.)

The apparent damage to a flashed 45° insulator is also consistent with Figs. 2 and 3. The damage is confined to the insulator surface and appears as a surface dendrite that originates at the anode junction [1,8–10,13,20,25]. The dendrite usually starts from a single point near the anode and branches toward the cathode. The branches, subbranches, etc., of a dendrite are approximately self similar, and a typical dendrite has a fractal geometry with a similarity dimension [53] on the order of $(\ln 12)/(\ln 5) = 1.5$. The dendritic branches extend toward the cathode, as pictured in Refs. [13,20,25].

A model of anode-initiated flashover has been developed by Anderson [8–10,13,25]. The model proposes that such a flashover initiates due to localized electron emission from the insulator surface. The emission might, for example, be due to field emission from particulates or other surface imperfections, or from the insulator material itself [1,8–10,13,25,45,46]. The model assumes that such emission brings a small region of the surface closer to the anode potential, increasing the electric field at the surface. When the field is sufficiently high, localized bulk-dielectric-breakdown events would occur at the surface. Since the electric field is highest at the anode triple junction, both electron emission and bulk breakdown would most likely initiate at this location.

Vacuum-diode experiments designed to measure electron emission from a flat PMMA insulator demonstrate that emission occurs at 0.4–0.5 MV/cm [13,54]. This is also the threshold electric field at which emission is observed from polyethylene, polyethylene terephthalate (Mylar), polyimide (Kapton), and other dielectrics [13]. As indicated by Table I, for voltage pulse widths on the order of a few seconds, bulk-dielectric breakdown of PMMA and Rexolite occurs at approximately 0.6 and 0.8 MV/cm, respectively. For time scales on the order of ~100 ns, bulk breakdown in PMMA and Rexolite occurs at 1.5–3.6 MV/cm [29,55]. (The dielectric-breakdown strength is expected to be reduced somewhat below these levels near the vacuum-insulator interface, due to imperfections in the bulk material at the interface.) Hence electron emission from the surface of a dielectric is expected to occur at fields below that required for bulk-dielectric failure.

Anderson proposes [8–10,13,25] that once it begins, anode-initiated flashover proceeds as follows: Dielectric-breakdown events on the insulator surface produce plasma that expands on the surface and into the vacuum. When the plasma comes into contact with the anode and is raised nearer to the anode potential, or when electron emission from the plasma brings it nearer to the anode potential, the electric field is increased at the edge of the expanding plasma on the surface. New generations of localized bulk breakdowns occur where the field exceeds the bulk breakdown strength of the insulator surface, and the discharge branches across the interface. The flashover is complete when the branch tips reach the cathode.

The Anderson model suggests at least three possible methods for improving the flashover strength of a 45° vacuum-insulator interface. The model predicts that:

(i) The flashover strength increases as ε is decreased, when the insulator geometry and all other insulator properties are held constant. (As indicated by Figs. 4 and 6, the electric-field magnitude E_m near the anode triple junction decreases as ε is decreased.)

(ii) The flashover strength increases as the bulk-dielectric-breakdown strength is increased, when the insulator geometry and all other insulator properties are held constant. (A higher bulk breakdown strength would make it more difficult to initiate and spread a discharge along the insulator surface.)

(iii) The flashover strength increases as the electric field near the anode triple junction is deenhanced, when ε and all other insulator properties are held constant.

E. Anode-plug calculations

As noted by McDaniel [47], Anderson [9], and Vogtlin and co-workers [20,22,26], the electric field near an anode triple junction can be deenhanced with an anode plug, i.e., an extension of the anode into the insulator.

Figure 7 illustrates an idealized plug that extends into a 45° insulator a depth $d/4$, and displays E_m as a function of position for this configuration. We present E_m since we expect that electron emission from the vacuum-insulator interface is determined by E_m on the vacuum side of the interface, and that bulk breakdown inside the insulator is also determined by E_m.

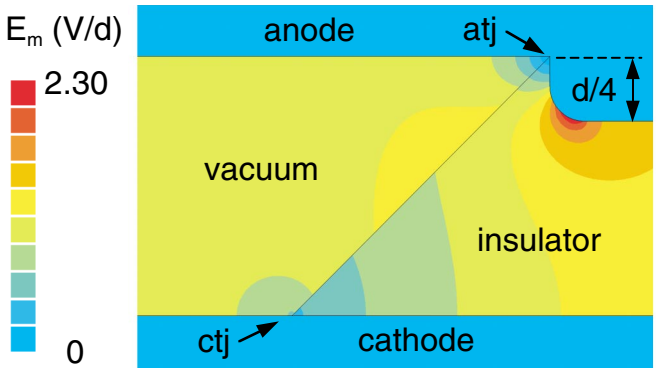

FIG. 7. (Color) The absolute value of the electric-field magnitude E_m as a function of position for an idealized 2D 45° vacuum-insulator interface with a $d/4$ anode plug. The figure assumes that the dielectric constant of the insulator $\varepsilon = 2.55$. The anode triple junction (atj) is the point at which the vacuum, insulator, and anode regions meet; the cathode triple junction (ctj) is similarly defined. The color legend is a linear scale. The field magnitude is given in units of V/d, where V is the voltage across the insulator and d is the insulator thickness as defined by Fig. 1. Comparing Figs. 2 and 7, it is clear that the plug decreases significantly the field at the anode triple junction.

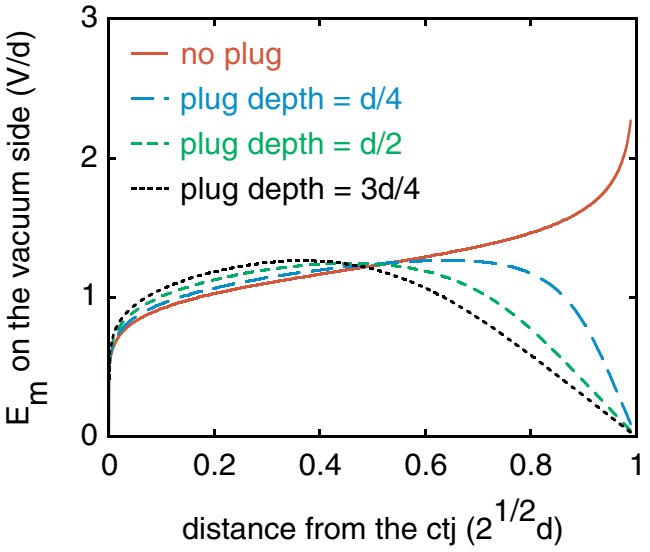

FIG. 8. (Color) The absolute value of the electric-field magnitude E_m on the vacuum side of an idealized 2D 45° vacuum-insulator interface, as a function of distance along the interface. The figure assumes that the dielectric constant of the insulator $\varepsilon = 2.55$. The field is plotted for four different anode-plug depths. [The plot for the case with no plug is identical to that labeled E_m (vac) in Fig. 3.] The field is given in units of V/d, where V is the voltage across the insulator and d is the insulator thickness as defined by Fig. 1. The distance from the ctj is given in units of $2^{1/2}d$, which is the total length of the vacuum-insulator interface.

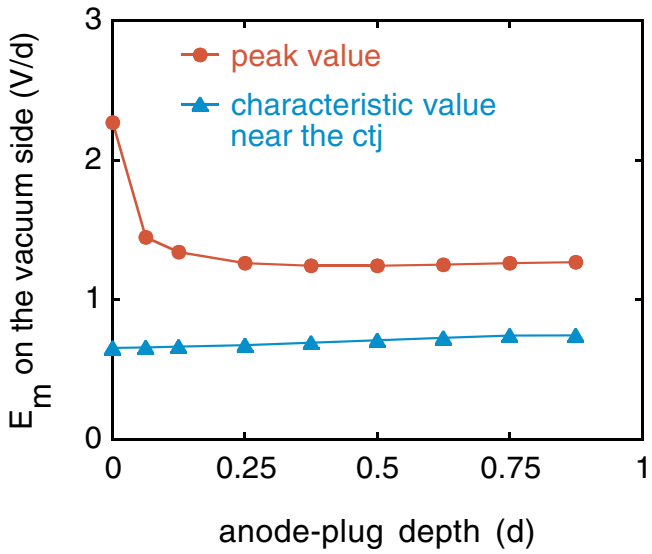

FIG. 9. (Color) The peak value of E_m on the vacuum side of an idealized 2D 45° vacuum-insulator interface, as a function of anode-plug depth. The figure assumes that the dielectric constant of the insulator $\varepsilon = 2.55$. (When the depth is equal to 0, we plot the characteristic value of E_m near the anode triple junction.) Also plotted is the characteristic value of E_m near the cathode triple junction. The fields are given in units of V/d, where V is the voltage across the insulator and d is the insulator thickness as defined by Fig. 1.

Figure 8 plots E_m as a function of distance along the vacuum-insulator interface, on the vacuum side, for 4 different anode-plug depths. [The plot for the case with no anode plug is identical to that labeled E_m (vac) in Fig. 3.] In Fig. 9 we plot the peak value of E_m on the vacuum side of the insulator surface as a function of plug depth. When there is no plug, we plot in Fig. 9 the characteristic value of E_m near the anode triple junction, as defined in Sec. II C. When the plug depth equals either $d/16$ or $d/8$, we assume that the radius at the edge of the plug equals the plug depth. When the depth is between $d/4$ and $7d/8$, we assume that the radius equals $2d/15$, to be consistent with the experiments discussed in Secs. III, IV, and V. (Figures 7–9 assume that the insulator and electrodes extend infinitely both into and out of the page, as do Figs. 2–6.)

As indicated by Figs. 2 and 7–9, an anode plug can significantly reduce the peak field on the surface of a 45° insulator. For the plug geometries considered here, the peak field is minimized for a plug depth between $d/4$ and $d/2$.

Of course, an anode plug improves the performance of an insulator-electrode system only when bulk-dielectric breakdown through the dielectric is much less likely to occur than flashover across the vacuum-insulator interface. The field in the bulk material increases as the depth of the plug is increased. The contour of the plug design depicted in Fig. 7 includes a simple radius; the peak field in the bulk material can be reduced substantially with a more complex shape.

As indicated by Figs. 8 and 9, increasing the plug depth beyond ~ $d/4$ does not significantly decrease the field on the insulator surface, whereas it substantially increases the field in the bulk material. Hence it appears that for a given application and set of constraints, an optimum plug depth exists that significantly deenhances the electric field at the anode triple junction while minimizing the electric-field magnitude in the bulk material. Figs. 8 and 9 suggest that the optimum depth is on the order of $d/4$.

III. EXPERIMENT

A. System configuration and procedures

Motivated by the Anderson model described in Sec. II D and the measurements performed by Milton [5,7], Vogtlin *et al.* [20,22,26], and Roth *et al.* [33], we have conducted a series of controlled flashover experiments to validate that the flashover strength of a 45° vacuum-insulator interface can be improved as indicated. We chose an angle of 45° because according to Smith [1] and Milton [5], this angle optimizes the flashover strength of a PMMA insulator, and according to Milton [5], 45° is also optimum for Rexolite. (In Ref. [5], Rexolite is referred to as C-Lecstyrene, and also as cross linked styrene.)

The experiments described below were conducted with insulators at least a factor of 2.7 thicker, and a factor of 6.4 larger in circumference, than those studied in Refs. [5,7,20,22,26,33]. We have also performed the first anode-plug experiments with a Rexolite insulator. Each insulator tested was in the shape of an axisymmetric ring; a cross-sectional view of a typical configuration used for the experiments is presented in Figs. 10 and 11.

The insulator thickness d (as defined by Fig. 1) was 4.318 cm. The circumference of the vacuum-insulator interface at the midplane was 95.74 cm. The anodes and cathodes were machined to a surface finish with a root-mean-square value of 0.3–0.6 μm; the insulators were machined to a finish of 0.6–1.0 μm. (These finishes were chosen because they are comparable to those which can be achieved for the components of a large-diameter insulator stack, such as the 3.3-m-diameter stack of the Z accelerator [36–44].) As discussed in Sec. III B, portions of the electrode surfaces were hard anodized [56] for some of the experiments. The thickness of the anodized coating was 25–51 μm; the root-mean-square value of the roughness of the anodized surfaces before the experiments was 1–2 μm. The surface finishes given here were validated with a profilometer; no other microscopic surface measurements were performed.

The experiments were conducted with no sources of charged particles or ultraviolet radiation except for those inherent to the insulator-electrode system itself when operated at high voltage. There was also no magnetic field except that due to the displacement current that charged the capacitance defined by the insulator and electrodes. This field was orders of magnitude less than that required for magnetic flashover inhibition [14,44].

The vacuum region indicated in Figs. 10 and 11 was evacuated with a 25.4-cm-diameter cryogenic vacuum pump for at least three hours before each shot. The inner surface of the insulator ring formed the vacuum-insulator interface. The insulator was not coated with oil or any other substance for the experiments. The outer insulator surface was in contact with water, used here as a high-voltage insulating medium. To inhibit the formation of a water arc, the axial thickness of the insulator on the water side of the insulator was thicker than on the vacuum side. (An earlier hardware design did not have this feature, and occasionally failed due to a water arc that severely cracked the insulator.) The water resistivity was approximately 15.5 ± 2.0 megahom-cm. Hermetic water-vacuum seals were made with ethylene-propylene O-rings with a nominal inner diameter of 38.1 cm (15 in.) and a nominal minor diameter of 0.476 cm (3/16 in.). The O-rings were covered

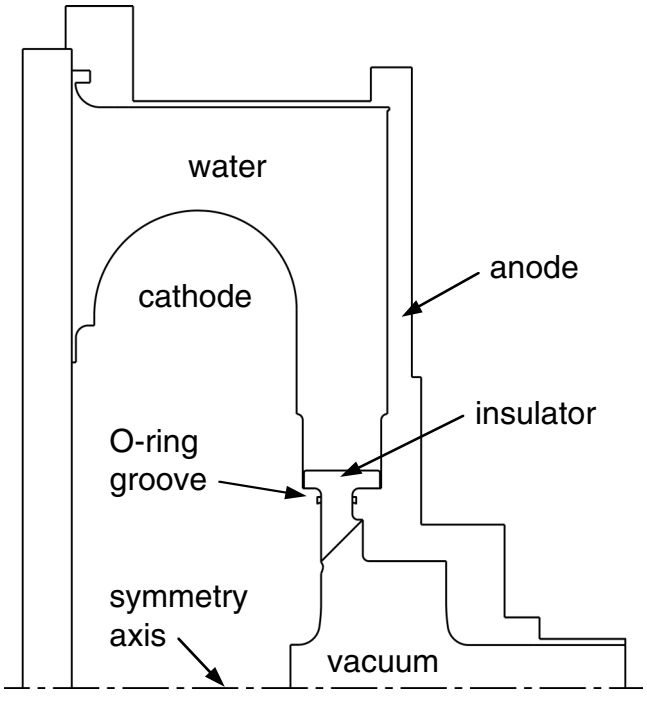

FIG. 10. Outline of the experimental arrangement. The hardware is cylindrically symmetric about the axis. The outer radius of the insulator is 22.48 cm.

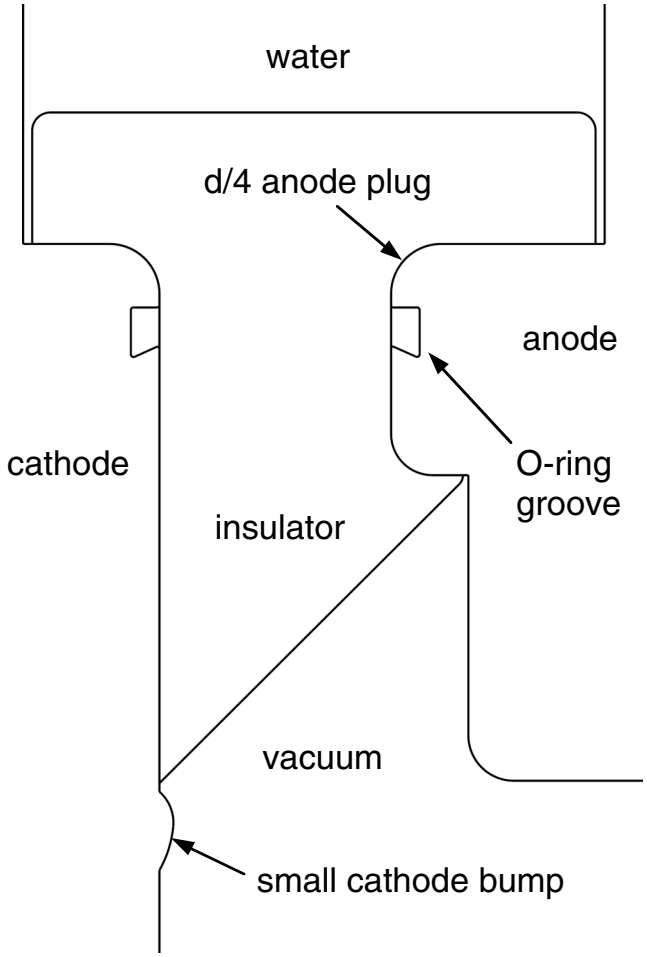

FIG. 11. Detail view of Fig. 10. The insulator-electrode geometry shown is that of configurations F, G, and H.

with a thin layer of Dow Corning silicon lubricant. The pressure in the vacuum region during a shot was 6.2×10^{-7}–1.3×10^{-5} torr.

Before going under vacuum, the measured gap at the cathode triple junction between the insulator and the cathode was ≤ 0.02 cm. On shots taken without an anode plug, the measured gap at the anode junction was ≤ 0.004 cm. On shots taken with a plug, the nominal gap at the anode junction was 0.076 cm. The anode-plug hardware was designed to produce such a gap to guarantee that the anode rested on the insulator at the anode-plug location, instead of at the sharp insulator corner at the anode triple junction.

The voltage pulse applied across an insulator was generated by the 1.2-ohm ZM accelerator [57]. When the accelerator's Marx charge voltage was 55 kV, the accelerator delivered a 2.2-MV pulse across the insulator, which was in effect an open-circuit load. Four dD/dt monitors measured the voltage across the insulator. The monitors were equally spaced azimuthally, located in the anode (nominally at ground potential) on the water side of the insulator, at a radial distance of 16.7 cm from the outer insulator surface. The monitors were calibrated *in situ* using an inductive short-circuit load and calibrated current monitors. A small correction to the monitor signals was performed to obtain the voltage across the insulator.

The damage to the insulator and electrodes caused by a single flashover, and the debris released, were substantial, since the current delivered to a flashover plasma was on the order of 1 MA. Hence the hardware could not be conditioned as it usually is for flashover measurements; i.e., the hardware could not be left under vacuum for repeated shots until stable flashover measurements were obtained. Instead, after each shot the anode and insulator were disassembled and removed from the accelerator. The anode, cathode, and insulator were cleaned with 280-, 400-, and 600-grit silicon-carbide sandpaper, class-10 clean-room towels, and ethyl alcohol filtered to remove particles with diameters greater than 0.2 μm. After reassembly, in preparation for a subsequent shot, the insulator and electrodes were dusted with an ionizing air gun (filtered to remove particles with diameters greater than 0.2 μm), and gaseous carbon dioxide from a hand-held pressurized canister.

Nine sets of measurements were performed, one for each of the nine insulator-electrode configurations that were tested. A new cathode, anode, and insulator were used at the beginning of each set of measurements.

B. Insulator-electrode configurations

The nine insulator-electrode configurations that were investigated are described in Table II and are labeled A through I. For each configuration except H, the anode and cathode were fabricated from aluminum alloy 6061-T6; configuration H used instead stainless steel 304L. Figure 10 illustrates the general hardware layout used for all the configurations. Figures 10 and 11 show the specific geometry used for configurations F, G, and H; the region indicated by Fig. 11 differed for the other configurations.

Configuration A is the standard 45° insulator-electrode system: a flat uncoated cathode (with no cathode bump); a flat uncoated anode (with no anode plug); and a 45° PMMA (acrylic-100M) insulator. Configuration B is identical to A except the insulator material for B is Rexolite 1422. The insulator-electrode geometry of configurations A and B is essentially that given by Fig. 1. It is also identical to Figs. 10 and 11, except that configurations A and B have neither an anode plug nor a cathode bump.

Configuration C is identical to B, except that for C, the entire anode and cathode surfaces exposed to vacuum were hard anodized [56]. We tested an anodized coating since it inhibits electron emission from the cathode at electric fields less than 300 kV/cm [58,59]. Configuration C also includes a small cathode bump, which slightly reduces the electric field near the cathode triple junction, and simulates the shape of a grading ring that might be used in the insulator stack of a pulsed-power accelerator. The cathode-bump geometry used is shown in Figs. 10 and 11.

Configuration D is identical to C, except D includes a larger cathode bump. The geometry of D, including that of the larger bump, is a 0.756-scale version of the insulator-electrode configuration used for the vacuum-insulator stack of the Z pulsed-power accelerator [36–44].

Configuration E is identical to B, except E includes a $d/4$ anode plug to reduce the electric field at the anode triple junction. The insulator-electrode geometry of E is identical to that given by Figs. 10 and 11, except that E does not include a cathode bump.

The geometry used for configurations F, G, and H is precisely that given by Figs. 10 and 11. F, G, and H have identical geometries but use different electrode materials. These were varied to determine if they have a significant effect on insulator flashover. For configuration F, part of the cathode was hard anodized [56]. The cathode was anodized from the symmetry axis shown in Fig. 10 to the outer edge of the cathode bump shown in Fig. 11, and was not anodized outside this edge. For configuration G, the entire anode and cathode surfaces exposed to vacuum were hard anodized. For configuration H, both the anode and cathode were fabricated from stainless steel, and were uncoated.

Configuration I is identical to F (and Figs. 10 and 11), except that for I, the anode-plug depth is $d/2$.

Figure 12 gives E_m as a function of position for the geometry outlined in Figs. 10 and 11, which is that of configurations F, G, and H. (The 25–51 μm thick anodized coating was not included in the electric-field calculation.) Figure 13 plots E_m as a function of distance along the vacuum side of the interface, for 6 of the 9 configurations. The fields for configurations C and D are similar to that of B, except that the C and D fields are somewhat lower near

TABLE II. Summary of insulator-flashover measurements. Each of these was obtained with an uncoated 45° polymethyl methacrylate (acrylic-100M) or crosslinked polystyrene (Rexolite-1422) insulator at a pressure $\leq 1.3 \times 10^{-5}$ torr. Aluminum alloy 6061-T6 was used for all of the aluminum electrodes; stainless steel 304L was used for configuration H. The flashover measurements were performed with no external sources of charged particles or ultraviolet radiation, and a magnetic field due only to the displacement current that charged the capacitance defined by the insulator and electrodes. The quantities $\overline{E_p}$, $t_{\rm eff}$ (nominal), $\gamma_{\rm SM}$, $\sigma(\gamma_{\rm SM})$, and $\sigma(X)$ are defined in Sec. III C. The values given for $\gamma_{\rm SM}$ assume E_p is expressed in kV/cm, $t_{\rm eff}$ in μs, and d, C in cm. For all these measurements $d = 4.318$ cm and $C = 95.74$ cm.

Hardware configuration label	Anode material	Anode geometry	Cathode material	Cathode geometry	Insulator material	Number of shots	$\overline{E_p}$ (kV/cm)	Nominal value of $t_{\rm eff}$ (μs)	$\gamma_{\rm SM}$	$\sigma(\gamma_{\rm SM})$	$\sigma(X)$
A	Aluminum	Flat	Aluminum	Flat	PMMA	19	265	0.0073	242	5%	(21 ± 4)%
B	Aluminum	Flat	Aluminum	Flat	Rexolite	28	293	0.0141	286	3%	(15 ± 2)%
C	Anodized aluminum	Flat	Anodized aluminum	Small bump	Rexolite	13	277	0.0090	258	5%	(18 ± 4)%
D	Anodized aluminum	Flat	Anodized aluminum	Large bump	Rexolite	13	282	0.0047	247	3%	(10 ± 2)%
Combined data for configurations B, C, and D						54	287	0.0099	270	2%	(16 ± 2)%
E	Aluminum	$d/4$ plug	Aluminum	Flat	Rexolite	13	426	0.0132	413	7%	(25 ± 5)%
F	Aluminum	$d/4$ plug	Partially anodized aluminum	Small bump	Rexolite	13	398	0.0105	377	8%	(30 ± 6)%
G	Anodized aluminum	$d/4$ plug	Anodized aluminum	Small bump	Rexolite	11	430	0.0070	391	4%	(13 ± 3)%
H	Stainless steel	$d/4$ plug	Stainless steel	Small bump	Rexolite	14	437	0.0136	424	6%	(23 ± 5)%
Combined data for configurations E, F, G, and H						51	423	0.0110	402	3%	(23 ± 2)%
I	Aluminum	$d/2$ plug	Partially anodized aluminum	Small bump	Rexolite	14	403	0.0073	368	7%	(24 ± 5)%

the cathode triple junction. The field for configuration E is similar to that of F, G, and H, except that the field for E is somewhat higher near the cathode junction.

C. Data analysis

Section II D reviews the Anderson model of anode-initiated flashover, which describes the *formative* component of the flashover process. Assuming that the characteristic *statistical* component of the flashover delay time is much greater than the flashover-plasma formation time, we can use the statistical-flashover model described in Ref. [36] to estimate the *probability* that a flashover occurs. The data are analyzed using this statistical model.

The statistical model predicts that for an applied unipolar voltage pulse $V(t)$, the flashover probability $f(t)$ of a single 45° insulator between *flat* electrodes is given by

$$f(t) = 1 - \exp\left(-\frac{E_p^{10} t_{\rm eff} C}{k^{10}}\right), \tag{4}$$

$$t_{\rm eff} \equiv \frac{1}{E_p^{10}} \int_0^t E^{10}(\tau)\, d\tau, \tag{5}$$

$$k \equiv \frac{\gamma_{\rm SM} \exp(0.24/d)}{(\ln 2)^{1/10}}. \tag{6}$$

The quantity $E_p \equiv V_p/d$ is the peak value in time of the mean electric field $E(t) \equiv V(t)/d$, V_p is the peak voltage in time across the insulator, d is the insulator thickness as defined by Fig. 1, C is the insulator circumference at the midplane of the vacuum-insulator interface, and $\gamma_{\rm SM}$ is a constant. Equation (6) assumes d is expressed in cm.

The flashover probability $f(t)$ equals 50% when

$$\frac{E_p (t_{\rm eff} C)^{1/10}}{\exp(0.24/d)} = \gamma_{\rm SM}. \tag{7}$$

Assuming E_p is expressed in kV/cm, $t_{\rm eff}$ in μs, and C, d in cm, the average value of the statistical-model constant $\gamma_{\rm SM} = 224 \pm 15$ for PMMA, and $\gamma_{\rm SM} \sim 248$ for

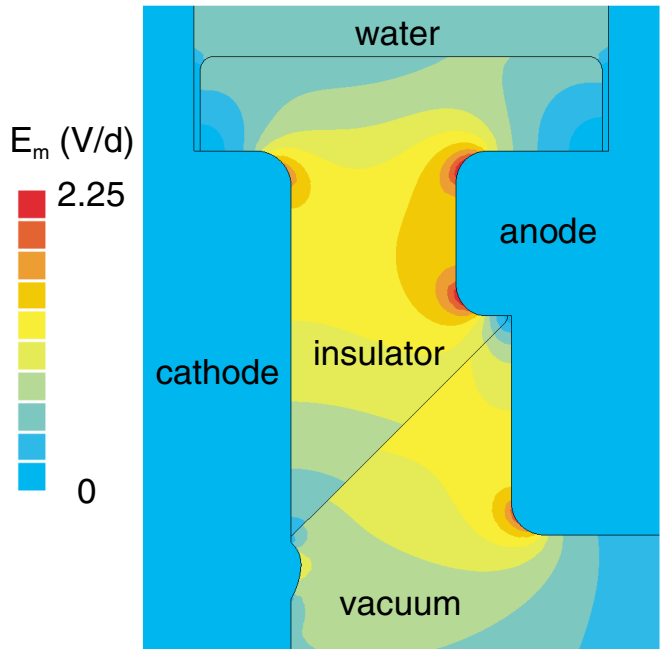

FIG. 12. (Color) The absolute value of the electric-field magnitude E_m as a function of position for the axisymmetric insulator-electrode configuration of Figs. 10 and 11. The field assumes that the dielectric constant of the insulator $\varepsilon = 2.55$. The color legend is a linear scale. The field is given in units of V/d, where V is the voltage across the insulator and d is the insulator thickness as defined by Fig. 1. The field plotted does not include effects due to the O-ring grooves shown in Figs. 10 and 11. A calculation with the grooves included shows that they change the peak value of E_m at the vacuum-insulator interface by 1%, and that the field very near the sharp corners of the grooves are on the order of $3V/d$. This assumes that the grooves are completely filled with ethylene propylene ($\varepsilon = 2.6$), the O-ring material.

Rexolite, for the measurements summarized in Table I of Ref. [36].

We define the *flashover strength* of an insulator to be the value of E_p at which the flashover probability equals 50%. Hence according to Eq. (7), when t_{eff}, C, and d are held constant, the flashover strength is proportional to γ_{SM}.

The statistical model given by Eqs. (4)–(7) was developed for a 45° insulator-electrode system assuming that the insulator material is either PMMA or Rexolite, with no anode plug. Under these conditions, the model appears to be valid when $100 \leq E_p \leq 651$ kV/cm, 0.5 ns $\leq t_{\text{eff}} \leq 10$ μs, $0.5 \leq d \leq 5.72$ cm, and $7.85 \leq C \leq 1003$ cm [36].

Presently an insufficient number of measurements have been performed to determine whether the model is applicable to an insulator that includes an anode plug. Until such measurements are available, we make the *tentative* assumption that Eqs. (4)–(7) apply to all 45° insulator-electrode systems considered in this article, and that only the constant γ_{SM} differs for the various configurations.

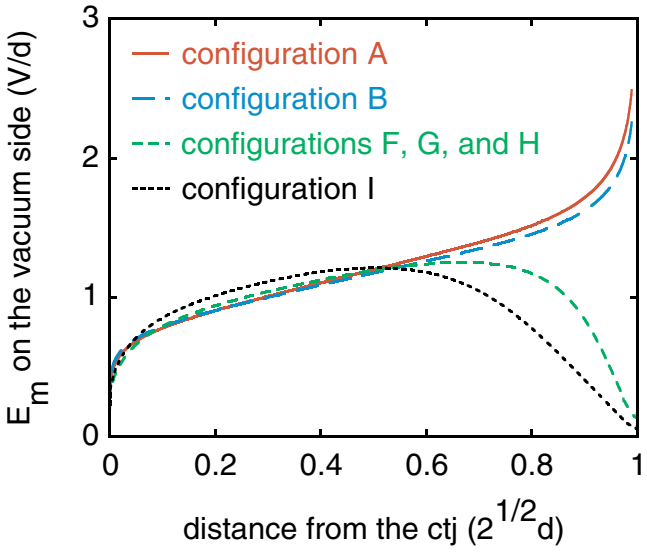

FIG. 13. (Color) The absolute value of the electric-field magnitude E_m on the vacuum side of the vacuum-insulator interface, as a function of distance along the interface, for 6 of the 9 configurations listed in Table II. (The fields for configurations C and D are similar to that of B, except that the C and D fields are somewhat lower near the cathode triple junction. The field for configuration E is similar to that of F, G, and H, except that the field for E is somewhat higher near the cathode junction.) The fields are given in units of V/d, where V is the voltage across the insulator and d is the insulator thickness as defined by Fig. 1. The distance from the ctj is given in units of $2^{1/2}d$, which is the total length of the vacuum-insulator interface.

At least 11 flashover measurements were performed for each of the 9 configurations listed in Table II. Typical insulator-voltage waveforms $V(t)$ for shots with and without an insulator flashover are plotted in Fig. 14.

We recorded $V(t)$ for each shot. From each waveform we obtain the peak electric field E_p that was achieved. We also

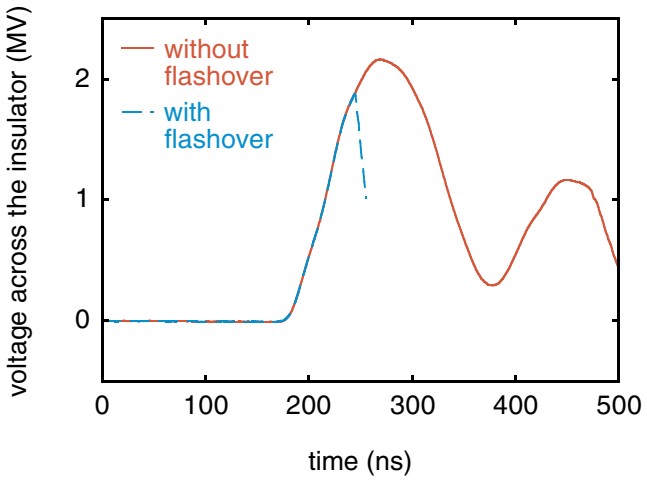

FIG. 14. (Color) Typical voltage pulses applied across an insulator for the flashover experiments.

obtain the effective width $t_{\rm eff}$ [defined by Eq. (5)] of the voltage pulse from $t = 0$ until the time at which $E(t) = E_p$. We use these values of E_p and $t_{\rm eff}$ to calculate for each shot the following quantity:

$$X \equiv \frac{E_p (t_{\rm eff} C)^{1/10}}{\exp(0.24/d)}. \quad (8)$$

For each of the 9 sets of measurements that were performed, we calculate $\overline{E_p}$ and $\overline{X}$, the mean values of E_p and X. For the cumulative flashover-distribution function given by Eq. (4), $\overline{X}$ and $\gamma_{\rm SM}$ are related as follows [60]:

$$\overline{X} = \frac{\Gamma[1 + (1/10)]}{(\ln 2)^{1/10}} \gamma_{\rm SM} = 0.987 \gamma_{\rm SM} \approx \gamma_{\rm SM}, \quad (9)$$

where Γ is the gamma function [61]. (Following Ref. [36], we ignore the factor of 0.987, and simply equate $\overline{X}$ with $\gamma_{\rm SM}$.) From Eq. (7), we obtain a nominal value of $t_{\rm eff}$, which we define as

$$t_{\rm eff}\ (\text{nominal}) \equiv \left[\frac{\gamma_{\rm SM} \exp(0.24/d)}{\overline{E}_p C^{1/10}} \right]^{10}. \quad (10)$$

The values of $\overline{E_p}$, $\gamma_{\rm SM}$, and $t_{\rm eff}$ (nominal) obtained in this manner are listed in Table II. We also list $\sigma(\gamma_{\rm SM})$, which is the standard deviation of the mean $\overline{X} \approx \gamma_{\rm SM}$, and $\sigma(X)$, the standard deviation in the values of X [49]. (These quantities are related by $\sigma(\gamma_{\rm SM}) = \sigma(X)/N^{1/2}$, where N is the number of measurements [49].)

As discussed in Sec. III A, we were unable to condition the insulator and electrode hardware as is normally done for flashover measurements. However, we did observe evidence of partial conditioning. As mentioned previously, a new set of hardware was used at the beginning of each of the 9 sets of measurements. We observed that the first shot in a set almost always produced a value of X somewhat lower than $\overline{X}$. We attribute this to sharp edges, machining lubricants absorbed at the hardware surfaces, inclusions in the insulator and electrode surfaces, and other fabrication artifacts, and have excluded such first-shot data from the analysis.

IV. RESULTS

The results of the experiments are summarized in Table II. Comparing the results obtained with configurations A and B, we find that the statistical-model constant $\gamma_{\rm SM}$ of Rexolite is $(18 \pm 7)\%$ higher than that of PMMA. This is within 2σ of the 9% value observed (on average) by Milton [5,7,36], and the 11% value obtained by Roth *et al.* [33]. Since these values differ by less than 2σ, they are not significantly different, and are consistent at a 95% confidence level [49]. Assuming the Anderson model of anode-initiated flashover, these results are also consistent with Figs. 4 and 6, and the electrical properties of Rexolite and PMMA listed in Table I.

As indicated by Figs. 4 and 6, the electric field near the cathode triple junction is *higher* for Rexolite than PMMA. Hence, if the flashover of a 45° insulator is most likely to initiate at the cathode triple junction, we would expect Rexolite to have a *lower* value of $\gamma_{\rm SM}$ than PMMA. Our observations contradict this, and instead support the Anderson model.

It appears that configurations C and D do not work as well as B. We believe this is due primarily to damage to the anodized coatings caused by the repeated flashovers of the experiments. New electrodes were used at the beginning of each set of measurements; however, during the course of each set of experiments conducted with an anodized coating on the cathode (or on both the cathode and anode), the coating became pitted near the cathode junction (or near both the cathode and anode junctions). The pitting occurred in an almost continuous ring around the entire circumference. It is possible, of course, that if an anodized coating is operated without being subjected to repeated megampere flashovers, and consequently without being severely pitted, the coating may not adversely affect the flashover performance of an insulator-electrode system. (Since an undamaged anodized coating inhibits electron emission [58,59], it may actually reduce the flashover probability.)

In the 5th row of Table II, we present results obtained by combining all the data taken with a 45° Rexolite insulator without a plug. Combining the data in this manner is meaningful only if the variations in the results obtained with configurations B, C, and D are not due to the differences in these configurations, but primarily to statistical fluctuations in the measurements.

Comparing configurations B and E, we find that a $d/4$ anode plug increases the statistical-model constant $\gamma_{\rm SM}$ of a 45° Rexolite insulator by $(44 \pm 11)\%$. This result is consistent (to within 2σ) with anode-plug experiments performed by Vogtlin, Hoflin, and Wilson [20]. These show that a 45° Lexan insulator with $d = 1$ cm, $C = 8.8$ cm, and an anode plug that extends a depth of 63% into the insulator does not flash when $E_p = 391$ kV/cm and $t_{\rm eff} = 0.067$ μs. Assuming the statistical-flashover model given by Eqs. (4)–(7), we estimate that $\gamma_{\rm SM}$ for this configuration is >292. This is $>38\%$ higher than the value of 211 that we infer for a 45° Lexan insulator without a plug. (We infer this value as follows: The average value of $\gamma_{\rm SM}$ for the 45° PMMA flashover measurements summarized in Table I of Ref. [36] is 224. These were obtained without an anode plug. From the data presented in Ref. [5], we estimate that the constant $\gamma_{\rm SM}$ for a 45° Lexan insulator without a plug is approximately 94% of that of PMMA. Multiplying 224 by this factor gives 211.)

Our results are also consistent with anode-plug experiments performed by Vogtlin and colleagues [20,22,26] with a PMMA insulator. These experiments were conducted with a 45° insulator with $d = 0.5$ cm,

$C = 10.37$ cm, and $t_{\text{eff}} = 0.836$ ns, with and without a 63% anode plug. The plug increased the nominal flashover strength from 522 kV/cm to more than 630 kV/cm, or by more than 21%. The insulator with a plug failed at 630 kV/cm due to bulk-dielectric breakdown, and not surface flashover, so a more accurate value of the improvement due to the plug was not recorded.

The results obtained with configurations B and E, and the measurements performed by Vogtlin *et al.* [20,22,26], are consistent with Figs. 2 and 7–9, which show that an anode plug substantially reduces the peak value of E_m at the vacuum-insulator interface. These observations are consistent with the Anderson model, and are inconsistent with a cathode-initiated-flashover mechanism.

The constants γ_{SM} for configurations E, F, G, and H, all of which include $d/4$ anode plugs, are the same to within the statistical uncertainties in γ_{SM}, i.e., to within 2σ. Hence it appears that the cathode bump and electrode materials tested in these systems do not have a significant effect on γ_{SM}. In the 10th row of Table II, we present results obtained by combining all the data taken with a 45° Rexolite insulator and a $d/4$ plug. We caution, however, that configurations F and G, both of which include an anodized coating, have slightly lower values of γ_{SM} than E and H, which is consistent with the trend observed with configurations B, C, and D.

The constant γ_{SM} for configuration I is comparable to that obtained with E, F, G, and H, which suggests that a $d/2$ plug performs approximately as well as a plug that extends a depth of $d/4$. Assuming the Anderson model, this observation is consistent with Figs. 8 and 9, which show that a $d/2$ plug reduces the peak value of E_m on the vacuum-insulator interface by only 1.5% below that achieved with a $d/4$ plug.

Although the $d/4$ and $d/2$ plugs have comparable flashover strengths (i.e., comparable values of the constant γ_{SM}), we observed a serious limitation of the $d/2$ design. On one of the shots taken with configuration I, the insulator failed catastrophically due to bulk-dielectric breakdown. Vogtlin and co-workers [20,22,26] also observed such bulk breakdowns with a $0.63d$ anode plug. We did not observe such a failure with a $d/4$ plug, although on 3 of the 51 shots taken at this plug depth, we observed the formation of a small dendrite in the bulk insulator material, near the anode-plug radius.

We note that assuming the cumulative flashover-probability distribution given by Eq. (4), the theoretical value of $\sigma(X)$, the standard deviation in the values of X [Eq. (8)], is calculated to be 12% [60]. This is an ideal limit and, as expected, is less than almost all the observed standard deviations listed in the 12th column of Table II. We believe that most of the observed deviations are greater than 12% because of shot-to-shot fluctuations in the following: (i) the conditioning of the hardware; (ii) damage to the hardware caused by the flashovers; (iii) the cleaning and refurbishment procedure (which was performed manually); (iv) the particulate content on the surfaces of the insulator and electrodes; (v) the roughness of these surfaces; and (vi) inclusions in these surfaces. We expect that flashover experiments conducted on an accelerator with an impedance substantially greater than 1.2 Ω would result in standard deviations closer to the theoretical value of 12%. Such experiments would cause less hardware damage, and would allow repeated flashover measurements to be performed without breaking vacuum and refurbishing the hardware between shots.

V. DISCUSSION

A. Rexolite and anode-plug limitations

As indicated by Table II, the statistical-model constant γ_{SM} of Rexolite is significantly greater than that of PMMA. Hence it appears that Rexolite would be a superior dielectric for use in the high-voltage vacuum-insulator interface of an accelerator.

Because of operational requirements, a vacuum-insulator interface may be routinely exposed to water vapor in air during cleaning. For some accelerators, the insulator that forms the vacuum-insulator interface also serves as the barrier between the accelerator's vacuum and water sections. Under such conditions, Rexolite would be expected to outgas more rapidly under vacuum than PMMA since (as indicated by Table I) Rexolite absorbs less water. We caution, however, that a Rexolite-water interface may have a weaker dielectric strength than a PMMA-water interface, since Rexolite does not ''wet'' as well.

Table II also suggests that an anode plug improves the performance of a 45° vacuum-insulator interface. Comparing the results obtained with configurations A and E, we find that in principle, a Rexolite insulator with a $d/4$ plug can increase the peak electromagnetic power that can be transmitted across a vacuum interface by a factor of approximately $(1.7)^2 = 2.9$ over that which can be achieved with the standard PMMA interface. Of course, such a gain can be realized only when other failure mechanisms (such as bulk dielectric failure of Rexolite, vacuum breakdown between the electrodes, etc.) can be prevented.

However, the use of anode plugs for a *large-diameter* insulator stack, such as the 3.3-m-diameter stack of the Z accelerator [36–44], presents some difficulties. The metal used for the plug is not likely to have the same thermal coefficient of expansion as Rexolite. (For example, the expansion coefficient of aluminum is approximately 2.5×10^{-5}/C, whereas for Rexolite it is $\sim 7 \times 10^{-5}$/C.) Hence a large radial gap would be required between the plug and insulator to accommodate the expected range of operating temperatures. Machining tolerances would further increase the size of the gap.

The radial gap used for the experiments described in this article was 0.076–0.178 mm. Assuming an aluminum plug, we estimate that a nominal gap on the order of 1.2 mm

would be required for a 3.3-m-diameter stack. This assumes a 10 °C temperature variation, and a ± 0.5 mm machining tolerance on the diameters of both the anode plug and Rexolite insulator.

Although numerical calculations show that a radial gap does not significantly affect the peak field at the 45° vacuum-insulator interface, such a gap may increase the probability of bulk-dielectric breakdown. For the geometry illustrated in Fig. 7, the characteristic electric field in a vacuum gap near the plug radius is on the order of $2.30\varepsilon V/d$, i.e., a factor of ε greater than the peak field plotted in the figure. If there is residual gas in the gap (due to material outgassing or the emission of electrons from the insulator), corona in the gas could erode the insulator and increase the probability of insulator failure. Additional experiments would be needed to characterize the performance as a function of the gap, and to develop an optimum vacuum-insulator design incorporating a gap significantly greater than the range tested.

B. Suggestions for future work

The results listed in Table II assume Eqs. (4)–(7) apply to the configurations incorporating an anode plug. The configurations tested all have the same insulator thickness d and circumference C; in addition, all the measurements were performed with the same value of t_{eff} (to within a factor of 3). We propose that experiments be conducted with larger values of d and C, and values of t_{eff} that differ significantly from those used for this study, to determine whether Eqs. (4)–(7) apply to an anode-plug configuration. We also suggest that *sample-to-sample* fluctuations [18,19,32] in the constant γ_{SM} be measured for insulator-electrode systems that include an anode plug.

In addition, it would be of interest to conduct experiments with novel insulator-electrode geometries, as described in Refs. [18,19,62,63], to explore whether flashover strengths greater than those obtained with an anode plug can be realized. The development and testing of new dielectric materials with values of ε lower than that of Rexolite, and with higher bulk-dielectric strengths, may also lead to improved flashover performance.

Moreover, we suggest that future flashover experiments be conducted on both high- and low-impedance accelerators. A high-impedance system delivers less current to a flashover plasma, and hence causes less damage to the insulator and electrodes. Because a high impedance causes less damage, it also permits a higher shot rate, which enables a reduction in the statistical uncertainties in the measurements. High-impedance experiments provide a direct assessment of vacuum interfaces designed to operate with little accumulated damage. Such experiments would complement those conducted on a low-impedance accelerator, as described in this article. A low-impedance machine delivers more current to a flashover, which causes more damage, but enables a realistic assessment of the performance of a vacuum interface expected to undergo repeated high-current flashovers.

ACKNOWLEDGMENTS

The authors would very much like to thank J. Boyes, H. Brown, P. Corcoran, J. Douglas, S. Drennan, T. Gilliland, D. Guthrie, M. Harris, K. Hodge, M. Horry, M. Johnson, R. Leeper, J. Lehr, F. Long, J. Maenchen, T. Martin, M. K. Matzen, R. Miller, O. Milton, M. Mostrom, T. Mulville, M. Navarro, J. Padilla, D. Petmecky, K. Prestwich, P. Reynolds, T. Romero, N. J. Rutledge, D. Sachs, J. Seamen, R. Shurter, I. Smith, J. Smith, C. Speas, B. Wood, O. Yamamoto, M. York, C-Lec Plastics, Continental Machine Shop, Esco Corporation, Ktech Corporation, Los Alamos National Laboratory, Mission Research Corporation, Prodyn Technologies, Team Specialty Products, Titan-Pulse Sciences Division, and Trace Laboratories for invaluable contributions. We are also extremely grateful to T. Cutler for graciously reviewing this article. Sandia is a multiprogram laboratory operated by Sandia Corporation, a Lockheed Martin Company, for the United States Department of Energy's National Nuclear Security Administration under Contract No. DE-AC04-94AL85000.

[1] I. D. Smith, in *Proceedings of the International Symposium on Insulation of High Voltages in Vacuum*, edited by J. G. Trump, R. P. Little, E. M. Lyman, and A. S. Denholm (Massachusetts Institute of Technology, Cambridge, MA, 1964), p. 261.
[2] W. R. Glock, master's thesis, Cornell University, 1969.
[3] W. R. Glock and S. Linke, Cornell University Laboratory of Plasma Studies Report No. LPS 24, 1969.
[4] J. C. Martin, Atomic Weapons Research Establishment High Voltage Note No. 2, SSWA/JCM/713/157, 1971.
[5] O. Milton, IEEE Trans. Electr. Insul. **7**, 9 (1972).
[6] C. H. de Tourreil and K. D. Srivastava, IEEE Trans. Electr. Insul. **8**, 17 (1973).
[7] O. Milton, Sandia National Laboratories Internal Memorandum, 25 April 1974.
[8] R. A. Anderson, in *Proceedings of the Conference on Electrical Insulation and Dielectric Phenomena, Gaithersburg, MD, 1975*, edited by the U. S. National Academy of Sciences (National Academy of Sciences, Washington, DC, 1978), p. 475.
[9] R. A. Anderson, Sandia National Laboratories Report No. SAND75-0667, 1976.
[10] R. A. Anderson, in *Proceedings of the VIIth International Symposium on Discharges and Electrical Insulation in Vacuum, Novosibirsk, USSR, 1976*, edited by the USSR Academy of Sciences, Siberian Branch (USSR Academy of Sciences, Novosibirsk, USSR, 1976), p. 252.
[11] A. A. Avdienko, Sov. Phys. Tech. Phys. **22**, 982 (1977).
[12] J. Golden and C. A. Kapetanakos, J. Appl. Phys. **48**, 1756 (1977).

[13] R. A. Anderson, in *Proceedings of the Conference on Electrical Insulation and Dielectric Phenomena, Whitehaven, PA, 1979*, edited by S. A. Boggs, C. M. Cooke, R. J. Densley, E. Sacher, and J. E. West (National Academy of Sciences, Washington, DC, 1979), p. 173.

[14] J. P. VanDevender, D. H. McDaniel, E. L. Neau, R. E. Mattis, and K. D. Bergeron, J. Appl. Phys. **53**, 4441 (1982).

[15] W. B. Moore, R. W. Stinnett, and D. H. McDaniel, in *Proceedings of the 5th IEEE Pulsed Power Conference, Arlington, VA, 1985*, edited by P. J. Turchi and M. F. Rose (IEEE, Piscataway, NJ, 1985), p. 315.

[16] M. A. Sweeney, in *Proceedings of the 5th IEEE Pulsed Power Conference, Arlington, VA, 1985*, edited by P. J. Turchi and M. F. Rose (IEEE, Piscataway, NJ, 1985), p. 319.

[17] W. K. Tucker, R. A. Anderson, and D. E. Hasti, in *Proceedings of the 5th IEEE Pulsed Power Conference, Arlington, VA, 1985*, edited by P. J. Turchi and M. F. Rose (IEEE, Piscataway, NJ, 1985), p. 323.

[18] N. C. Jaitly and T. S. Sudarshan, in *Proceedings of the 6th IEEE Pulsed Power Conference, Arlington, VA, 1987*, edited by B. H. Bernstein and P. J. Turchi (IEEE, Piscataway, NJ, 1987), p. 64.

[19] N. C. Jaitly and T. S. Sudarshan, IEEE Trans. Electr. Insul. **22**, 801 (1987).

[20] G. E. Vogtlin, W. W. Hofer, and M. J. Wilson, Lawrence Livermore National Laboratory UCRL Report No. 98704, 1988.

[21] O. Yamamoto, T. Hara, T. Nakae, and I. Ueno, in *Proceedings of the XIIIth International Symposium on Discharges and Electrical Insulation in Vacuum, Paris, 1988*, edited by J. M. Buzzi and A. Septier (Conservatoire National des Arts et Métiers, Paris, 1988), p. 250.

[22] G. E. Vogtlin and J. E. Vernazza, in *Proceedings of the 7th IEEE Pulsed Power Conference, Monterey, CA, 1989*, edited by R. White and B. H. Bernstein (IEEE, Piscataway, NJ, 1989), p. 808.

[23] O. Yamamoto, T. Hara, T. Nakae, and M. Hayashi, IEEE Trans. Electr. Insul. **24**, 991 (1989).

[24] O. Yamamoto, T. Hara, T. Nakae, I. Ueno, and M Hayashi (unpublished).

[25] R. A. Anderson, in *Proceedings of the XIVth International Symposium on Discharges and Electrical Insulation in Vacuum, Santa Fe, NM, 1990*, edited by R. W. Stinnett (Sandia National Laboratories, Santa Fe, NM, 1990), p. 311.

[26] G. E. Vogtlin, in *Proceedings of the XIVth International Symposium on Discharges and Electrical Insulation in Vacuum, Santa Fe, NM, 1990* (Ref. [25]), p. 307.

[27] O. Yamamoto, T. Hara, I. Nakanishi, and M. Hayashi, in *Proceedings of the XIVth International Symposium on Discharges and Electrical Insulation in Vacuum, Santa Fe, NM, 1990* (Ref. [25]), p. 400.

[28] O. Yamamoto, T. Hara, K. Ohmae, and M. Hayashi, Denki Gakkai Ronbunshi **110-A**, 830 (1990) [Electr. Eng. Jpn. **112**, 11 (1992)].

[29] R. P. Shurter, R. L. Carlson, and J. G. Melton, in *Proceedings of the 9th IEEE International Pulsed Power Conference, Albuquerque, NM, 1993*, edited by K. R. Prestwich and W. L. Baker (IEEE, Piscataway, NJ, 1993), p. 249.

[30] O. Yamamoto, T. Hara, H. Matsuura, M. Hayashi, and K. Yukimura, in *XVIth International Symposium on Discharges and Electrical Insulation in Vacuum, Moscow–St. Petersburg, 1994*, edited by G. A. Mesyats, Proc. SPIE Int. Soc. Opt. Eng. Vol. 2259 (SPIE-International Society for Optical Engineering, Bellingham, WA, 1994), p. 354.

[31] J. C. Martin, in *J. C. Martin on Pulsed Power*, edited by T. H. Martin, A. H. Guenther, and M. Kristiansen (Plenum Press, New York, 1996), p. 255.

[32] I. D. Smith, IEEE Trans. Plasma Sci. **25**, 293 (1997).

[33] I. S. Roth, P. S. Sincerny, L. Mandelcorn, M. Mendelsohn, D. Smith, T. G. Engel, L. Schlitt, and C. M. Cooke, in *Proceedings of the 11th IEEE International Pulsed Power Conference, Baltimore, MD, 1997*, edited by G. Cooperstein and I. Vitkovitsky (IEEE, Piscataway, NJ, 1997), p. 537.

[34] J. M. Elizondo, A. J. Dragt, M. Krogh, B. Stygar, K. Struve, R. Spielman, and K. R. Prestwich, in *Proceedings of the 13th IEEE International Pulsed Power Conference, Las Vegas, 2001*, edited by R. Reinovsky and M. Newton (IEEE, Piscataway, NJ, 2001), p. 1810.

[35] O. Yamamoto, T. Takuma, Y. Kakehashi, S. Ikoma, A. Nishimoto, and T. Iida, in *Proceedings of the XIXth International Symposium on Discharges and Electrical Insulation in Vacuum, Xi'an, China, 2000*, edited by Xi'an Jiaotong University (Xi'an Jiaotong University, Xi'an, China, 2000), p. 108.

[36] W. A. Stygar, H. C. Ives, T. C. Wagoner, J. A. Lott, V. Anaya, H. C. Harjes, J. P. Corley, R. W. Shoup, D. L. Fehl, G. R. Mowrer, Z. R. Wallace, R. A. Anderson, J. D. Boyes, J. W. Douglas, M. L. Horry, T. F. Jaramillo, D. L. Johnson, F. W. Long, T. H. Martin, D. H. McDaniel, O. Milton, M. A. Mostrom, D. A. Muirhead, T. D. Mulville, J. J. Ramirez, L. E. Ramirez, T. M. Romero, J. F. Seamen, J. W. Smith, C. S. Speas, R. B. Spielman, K. W. Struve, G. E. Vogtlin, D. E. Walsh, E. D. Walsh, M. D. Walsh, and O. Yamamoto, Phys. Rev. ST Accel. Beams **7**, 070401 (2004).

[37] R. B. Spielman, W. A. Stygar, J. F. Seamen, F. Long, H. Ives, R. Garcia, T. Wagoner, K. W. Struve, M. Mostrom, I. Smith, P. Spence, and P. Corcoran, in *Proceedings of the 11th IEEE International Pulsed Power Conference, Baltimore, MD, 1997* (Ref. [33]), p. 709.

[38] H. C. Ives, D. M. Van De Valde, F. W. Long, J. W. Smith, R. B. Spielman, W. A. Stygar, R. W. Wavrick, and R. W. Shoup, in *Proceedings of the 11th IEEE International Pulsed Power Conference, Baltimore, MD, 1997* (Ref. [33]), p. 1602.

[39] M. A. Mostrom, T. P. Hughes, R. E. Clark, W. A. Stygar, and R. B. Spielman, in *Proceedings of the 11th IEEE International Pulsed Power Conference, Baltimore, MD, 1997* (Ref. [33]), p. 460.

[40] R. W. Shoup, F. Long, T. H. Martin, R. B. Spielman, W. A. Stygar, M. A. Mostrom, K. W. Struve, H. Ives, P. Corcoran, and I. Smith, in *Proceedings of the 11th IEEE International Pulsed Power Conference, Baltimore, MD, 1997* (Ref. [33]), p. 1608.

[41] I. D. Smith, P. A. Corcoran, W. A. Stygar, T. H. Martin, R. B. Spielman, and R. W. Shoup, in *Proceedings of the 11th IEEE International Pulsed Power Conference, Baltimore, MD, 1997* (Ref. [33]), p. 168.

[42] W. A. Stygar, R. B. Spielman, G. O. Allshouse, C. Deeney, D. R. Humphreys, H. C. Ives, F. W. Long, T. H. Martin, M. K. Matzen, D. H. McDaniel, C. W. Mendel, Jr., L. P. Mix, T. J. Nash, J. W. Poukey, J. J. Ramirez, T. W. L. Sanford, J. F. Seamen, D. B. Seidel, J. W. Smith, D. M. Van De Valde, R. W. Wavrik, P. A. Corcoran, J. W. Douglas, I. D. Smith, M. A. Mostrom, K. W. Struve, T. P. Hughes, R. E. Clark, R. W. Shoup, T. C. Wagoner, T. L. Gilliland, and B. Peyton, in *Proceedings of the 11th IEEE International Pulsed Power Conference, Baltimore, MD, 1997* (Ref. [33]), p. 591.

[43] W. A. Stygar, R. B. Spielman, R. A. Anderson, R. E. Clark, J. W. Douglas, T. L. Gilliland, M. L. Horry, T. P. Hughes, H. C. Ives, F. W. Long, T. H. Martin, D. H. McDaniel, O. Milton, M. A. Mostrom, J. F. Seamen, R. W. Shoup, J. W. Smith, K. W. Struve, G. E. Vogtlin, T. C. Wagoner, and O. Yamamoto, in *Proceedings of the 12th IEEE International Pulsed Power Conference, Monterey, CA, 1999*, edited by C. Stallings and H. Kirbie (IEEE, Piscataway, NJ, 1999), p. 454.

[44] M. E. Savage, W. A. Stygar, J. M. Elizondo, H. C. Ives, W. Shoup, K. W. Struve, and D. H. McDaniel, in *Proceedings of the 26th International Power Modulator Symposium and 2004 High Voltage Workshop, San Francisco, CA, 2004*, edited by IEEE (IEEE, Piscataway, NJ, 2004), p. 54.

[45] A. Watson, J. Appl. Phys. **38**, 2019 (1967).

[46] K. D. Bergeron and D. H. McDaniel, Appl. Phys. Lett. **29**, 534 (1976).

[47] D. H. McDaniel (unpublished).

[48] Integrated Engineering Software, Winnipeg, Manitoba, Canada.

[49] J. R. Taylor, *An Introduction to Error Analysis* (University Science, Sausalito, California, 1997).

[50] J. P. Brainard, in *Proceedings of the Conference on Electrical Insulation and Dielectric Phenomena, Gaithersburg, MD, 1975* (Ref. [8]), p. 482.

[51] L. Schächter, Appl. Phys. Lett. **72**, 421 (1998).

[52] M. S. Chung, B-G. Yoon, P. H. Cutler, and N. M. Miskovsky, J. Vac. Sci. Technol. B **22**, 1240 (2004).

[53] B. B. Mandelbrot, *The Fractal Geometry of Nature* (W. H. Freeman and Company, New York, 2000).

[54] G. B. Frazier (unpublished).

[55] R. P. Shurter (private communication).

[56] The hard anodizing of the aluminum electrodes was performed according to the following specifications: MIL-A-8625E, type III, class I, no color, no seal, (0.001–0.002) in. thick, with a light caustic pre-etch that removed (0.0001–0.0002) in. of aluminum before anodizing.

[57] H. C. Harjes, J. P. Corley, J. A. Lott, V. Anaya, S. A. Drennan, D. W. Guthrie, K. C. Hodge, H. C. Ives, T. J. Jaramillo, D. L. Johnson, D. H. McDaniel, G. R. Mowrer, D. A. Muirhead, M. J. Navarro, J. J. Ramirez, L. E. Ramirez, K. W. Struve, W. A. Stygar, and T. C. Wagoner, Sandia National Laboratories Report No. SAND2003-0592A, 2003.

[58] G. B. Frazier, Physics International Company Report No. PIFR-784, 1975.

[59] G. B. Frazier, in *Proceedings of the 2nd IEEE International Pulsed Power Conference, Lubbock, TX, 1979*, edited by A. H. Guenther and M. Kristiansen (IEEE, Piscataway, NJ, 1979), p. 127.

[60] K. C. Kapur and L. R. Lamberson, *Reliability in Engineering Design* (Wiley, New York, 1977).

[61] M. Abramowitz and I. A. Stegun, *Handbook of Mathematical Functions* (Dover, New York, 1972).

[62] G. A. Tripoli, D. Conte, S. W. Seiler, P. J. Turchi, and C. N. Boyer, in *Proceedings of the 7th IEEE International Pulsed Power Conference, Monterey, CA, 1989*, edited by R. White and B. H. Bernstein (IEEE, Piscataway, NJ, 1989), p. 820.

[63] J. D. Smith, D. J. Kahaian, E. M. Honig, R. E. Montoya, L. A. Rosocha, G. R. Allen, and W. F. Aaron III, in *Proceedings of the 8th IEEE International Pulsed Power Conference, Monterey, CA, 1991*, edited by K. Prestwich and R. White (IEEE, Piscataway, NJ, 1991), p. 882.